

Reliability of numerical computation of pedestrian-level wind environment around a row of tall buildings

K. M. Lam[†]

Department of Civil Engineering, University of Hong Kong, Pokfulam Road, Hong Kong

A. P. To[‡]

*Ove Arup & Partners Hong Kong Limited, 5/F, Festival Walk,
Tat Chee Avenue, Kowloon Tong, Hong Kong*

(Received October, 10, 2005, Accepted October 23, 2006)

Abstract. This paper presents numerical results of pedestrian-level wind environment around the base of a row of tall buildings by CFD. Four configurations of building arrangement are computed including a single square tall building. Computed results of pedestrian-level wind flow patterns and wind speeds are compared to previous wind tunnel measurement data to enable an assessment of CFD predictions. The CFD model uses the finite-volume method with RNG $k-\varepsilon$ model for turbulence closure. It is found that the numerical results can reproduce key features of pedestrian-level wind environment such as corner streams around corners of upwind building, sheltered zones behind buildings and channeled high-speed flow through a building gap. However, there are some differences between CFD results and wind tunnel data in the wind speed distribution and locations of highest wind speeds inside the corner streams. In locations of high ground-level wind speeds, CFD values match wind tunnel data within $\pm 10\%$.

Keywords: CFD; pedestrian-level winds; wind environment; building interaction.

1. Introduction

Environmental wind conditions on the ground level are related to comfort and safety of pedestrians passing around tall buildings (Isyumov and Davenport 1975, Melbourne 1978). Evaluation of pedestrian-level wind environment has almost become a standard step in design of tall building developments. The traditional tool for evaluation is ad-hoc wind tunnel testing in which ground-level wind speeds are measured with hot-wires or special probes (Melbourne and Jourbert 1971, Irwin 1981). Whole-field measurement techniques have been reported using the scour technique (Livesey, *et al.* 1992) and other non-conventional methods (Sasaki, *et al.* 1992). There have also been some generic studies on pedestrian-level wind environment around tall buildings of systematically varied geometries and features (Stathopoulos and Storms 1986, Uematsu, *et al.* 1992,

[†] Associate Professor, Corresponding Author, E-mail: kmlam@hku.hk

[‡] Wind Engineering Consultant

To and Lam 1995a,b, Stathopoulos and Wu 1995).

Computational fluid dynamics (CFD) has been increasingly applied to investigate wind flow around buildings (Paterson and Apelt 1986, Zhou and Stathopoulos 1997). A study by Architectural Institute of Japan (AIJ) a few years back concluded that prediction of wind loads by CFD gains some successes for low-rise buildings (Tamura, *et al.* 1997, AIJ 1998). Assessment of wind loads on tall buildings by CFD is still not yet accepted by wind engineers. There is, however, much less reservation of the wind engineering community to accept CFD as a tool to investigate wind flow patterns around buildings with applications to ventilation study, dispersion modeling and assessment of pedestrian-level wind environment (Straw, *et al.* 2000, Meroney, *et al.* 1999, Ferreira, *et al.* 2002).

The challenge of CFD in computation of wind flow around buildings is on turbulence modeling. The k - ε model or other forms of Reynolds averaged Navier-Stokes equation (RANS) methods has been the standard closure method in commercial and some research CFD codes (Paterson and Apelt 1986, Ferreira, *et al.* 2002). The AIJ study suggested that these models are generally satisfactory in the prediction of time-averaged wind flow pattern over a low-rise building (Tamura, *et al.* 1997, AIJ 1998). More complex treatments of turbulence closure by the large eddy simulation (LES) and direct numerical simulation (DNS) have been used in some CFD studies of wind engineering problems (He and Song 1999, Murakami 1998).

In recent years, some works have been reported on the application of CFD to prediction of pedestrian-level wind environment (Ferreira, *et al.* 2002, He and Song 1999). Investigations were mostly on a particular building development and it is hard to generalize the results to other building projects. In many studies, only CFD results were reported and no experimental data are available for comparison. It is encouraging to note that AIJ is currently carrying out a comprehensive comparison study between CFD and wind tunnel measurements on pedestrian-level wind environment around a variety of building configurations (Yoshie, *et al.* 2005a,b, Tominaga, *et al.* 2005).

In this paper, pedestrian-level wind environment around a generic tall building and around two of these building placed side-by-side is computed by CFD using RNG (Re-Normalization Group) k - ε model. The building geometries and computational conditions are set to be identical to wind-tunnel experiments carried out previously by the writers (To and Lam 1995a,b). This enables direct comparison between CFD prediction and wind tunnel data. We hope to reflect the degree of confidence to which the more industrial-standard RANS-based CFD can assess pedestrian-level wind environment around a tall building or a group of tall buildings.

2. Wind tunnel experiment

Experimental results on pedestrian-level wind environment around a row of tall buildings have been obtained from wind tunnel tests carried out by the writers (To and Lam 1995a,b). Experiments were carried out in the boundary layer wind tunnel of Department of Civil Engineering at the University of Hong Kong. The configuration studied in To and Lam (1995a) was a row of four identical tall buildings arranged side-by-side with clear separation between adjacent buildings at one building breadth. Measurements were performed on three building configurations, Cases I to III, which are shown in Fig. 1. The model buildings were $H=37.5$ cm tall and had a square plan of breadth $B=15$ cm. Targeted geometric scale was 1:200 and full-scale building size was 75 m tall and 30 m wide. Ground-level wind speeds were measured by a split-fibre hot-wire probe at a height 1 cm above wind tunnel floor. This height corresponded to 2 m full-scale which was the standard

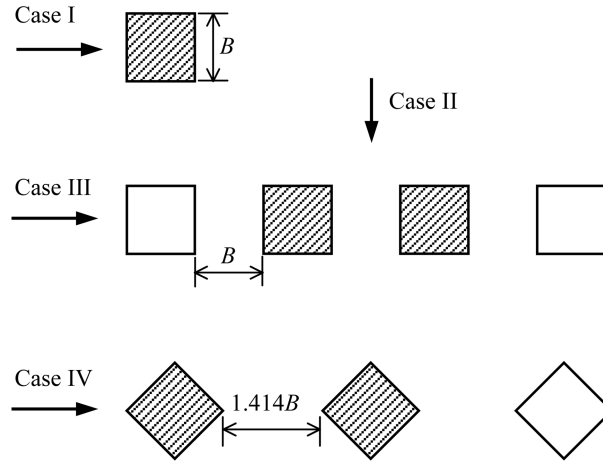


Fig. 1 Flow cases for wind tunnel tests and CFD (shaded building models only)

height for evaluation of pedestrian-level wind environment. It is worth noting that the split-fibre hot-wire was also used in the very recent study of AIJ to measure ground-level wind vectors in the wind tunnel (Yoshie, *et al.* 2005a,b). Another building configuration was tested and reported in To and Lam (1995b). In this Case IV (Fig. 1), ground-level wind speeds were measured with a single hot-wire probe. The hot-wire sensor was located vertically to measure only magnitude of the velocity vector regardless of flow direction.

The wind tunnel testing section was 3 m wide and 1.8 m high. Wind characteristics measured in the wind tunnel have been reported in To and Lam (1995a) and they simulated natural wind over open exposure terrain at a 1:200 scale. This terrain type was chosen because rows of identical tall buildings are often found for residential developments located along a coastline or harbor front in rather exposed sites. Measured profile of mean velocity followed well the power law with exponent 0.15:

$$\frac{U(z)}{U_H} = \left(\frac{z}{H}\right)^{0.15}, \quad z < 1.5 \text{ m} \quad (1)$$

with undisturbed wind speed at building roof height at $U_H=11.0$ m/s. Above $z=1.5$ m, $U(z)$ remained fairly constant. Along-wind turbulence intensity had values $I_u \approx 0.20$ near ground and $I_u \approx 0.10$ above 1.5 m height. In this paper, we chose to describe the measured profile with the power law and the best-fit equation was:

$$I_u(z) = \frac{\sigma_u(z)}{U(z)} = 0.143 \times \left(\frac{z}{H}\right)^{-0.20}, \quad z < 1.5 \text{ m} \quad (2)$$

σ_u being along-wind root-mean-square (r.m.s.) velocity fluctuations.

3. Numerical model

3.1. CFD code and computational domain

Wind flow around building models in the wind tunnel was computed using a CFD code, FLUENT (Fluent Inc. 2003). The code used the finite volume method to solve three-dimensional,

incompressible steady-state continuity and momentum equations (Patankar 1980). The equations were Reynolds-averaged and the k - ε method was used for turbulence closure. The Re-Normalization Group (RNG) extension (Yakhot and Orszag 1986) of k - ε model was adopted because of its capacity to better model flows with strongly curving streamlines or recirculating flows (Ferreira, *et al.* 2002). Flow equations and closure equations were solved to obtain steady-state solutions of the six flow variables, namely, pressure, the three velocity components, turbulent kinetic energy k and turbulence dissipation rate ε . The solution scheme made use of SIMPLEC algorithm (Van Doormaal and Raithby 1984) for pressure-velocity coupling and QUICK scheme (Leonard 1979) for convective transport modelling. Convergence of solutions was normally achieved after about 3000 iterations.

Computations were carried out on four test cases of building arrangements. They corresponded to Cases I to IV of wind tunnel study but only two buildings were used in a row (Fig. 1). This was because the wind tunnel tests showed that effects on environmental wind conditions of a building being located in a row were largely confined to the first two building members in Case III and Case IV. In Case II, the effects were mainly observed in the gap between two buildings (To and Lam 1995a). Using two buildings only could largely reduce the number of computational cells.

The computational domain represented a section of the wind tunnel. It had the same cross-sectional size of 3 m width and 1.8 m height. Cartesian coordinate system (x, y, z) aligned with the wind axes was used with the origin at the center of the first tall building (or center of building gap in Case II). The length of domain was set at 6 m covering $x = -1.5$ m to 4.5 m. In terms of building height, the computational domain covered an upwind fetch of $4H$ and a downwind fetch of $12H$. The height of domain was $4.8H$ and the width was $y = \pm 4H$. This domain size has been found to be sufficient to model flow around a tall building with a square plan (Lu, *et al.* 2001). Although the flow geometry was symmetrical about the x - z plane, full flow section was simulated. This did not allow reduction of the number of computational cells by a half but could provide an additional check for convergence of the steady-state flow solution which should exhibit symmetrical patterns about the x - z plane.

A large number of computational cells, $120 \times 90 \times 80$, $120 \times 120 \times 80$, $150 \times 90 \times 80$, and $195 \times 80 \times 80$ (in x - y - z directions), respectively in Cases I to IV, were used to discretize the flow domain. A non-uniform rectangular grid system was used. In the vertical direction, region from the ground up to height $z = H$ was divided into 40 cells with decreasing mesh sizes going towards both directions (Fig. 2a). Near the ground, there were four vertical computational cells below the plane $z = 1$ cm for evaluation of pedestrian-level wind environment. Another 40 cells were used to model the region from $z = H$ up to the top of computational domain. On the horizontal plane, in regions normal to the buildings or building gap, one building breadth was modeled with 20 cells (Fig. 2b). Along the x direction, there were 30 cells upwind of the building or building row and 60 to 70 cells downwind.

3.2. Boundary conditions

For direct comparison with experimental results in To and Lam (1995a,b), flow entering into the computational domain was set with boundary conditions matching wind characteristics in the wind tunnel. Profiles of mean wind speed $U(z)$ and along-wind turbulence intensity $I_u(z)$ following Eqs. (1) and (2) were used to set the inlet velocity conditions. Mean velocities in other directions were set to zero, that is $V = W = 0$. R.m.s. velocity fluctuations in the across-wind and vertical directions were taken as the following fixed ratios to σ_u :

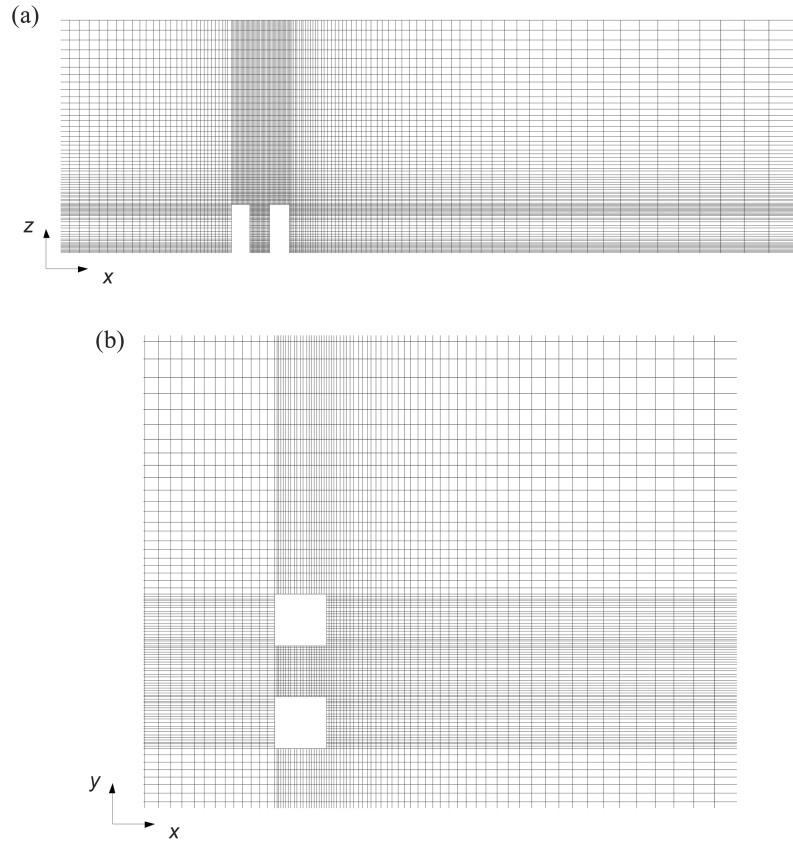


Fig. 2 Set up of computational grid. (a) Case III; (b) Case II

$$\begin{aligned} \sigma_v &= 0.7 \sigma_u \\ \sigma_w &= 0.5 \sigma_u \end{aligned} \tag{3}$$

In k - ε model, turbulence boundary conditions at inlet plane were imposed in terms of turbulent kinetic energy k and turbulence dissipation rate ε . They were calculated from:

$$k(z) = \frac{1}{2}(\sigma_u^2 + \sigma_v^2 + \sigma_w^2) = 0.87(UI_u)^2 \tag{4}$$

and

$$\varepsilon = \frac{C_\mu^{3/4} k^{3/2}}{0.4z} \tag{5}$$

Standard value of model constant at $C_\mu=0.0845$ for the RNG k - ε method was used. All flow entering into the computational domain was made to flow out at the downstream end with the outflow boundary condition. For Case I, we had carried out CFD computation using a number of inlet velocity boundary conditions to observe the sensitivity of computation results to different profiles of mean wind speed and turbulence intensity.

The symmetry boundary condition which simulated free field condition was used for the top and

two vertical sides of computation domain. Computations had also been attempted with the solid wall boundary condition for these walls and nearly identical computation results were found. The bottom of domain corresponded to the wind tunnel floor and was set as a solid wall. Standard wall functions were used and a value of $z_o=0.125$ cm was used for the aerodynamic roughness length. Several values had been tried and this value was found to best model the equilibrium boundary layer flow through the computational domain without any building. We actually found that computational results were largely insensitive to changes in z_o value by a factor of two from our chosen value. When translated to full scale, the chosen value of z_o corresponds to 0.25 m which seems to be on the high side for open terrain. However, the wall function used in the FLUENT code is based on flow inside rough-walled pipes and z_o is actually the equivalent sand-grain roughness. It is common that a 5 to 10 times multiple of sand-grain roughness is required in RANS-based CFD to model the aerodynamic roughness length in an atmospheric boundary layer. All building walls were set as solid walls with $z_o=0.05$ cm. Again, sensitivity test had been carried out on this value of z_o and we found that the flow is almost totally insensitive to this parameter. This is expected because wind flow over buildings is a turbulent separated flow where wall roughness does not play an important role.

4. Results and discussion

Before computation of Cases I to IV of wind flow around tall buildings, two reference flow situations were computed first to validate the numerical model including CFD code, grid set up and boundary conditions. The first flow was an empty flow domain the same as Case I but without presence of any building. The purpose was to check whether the boundary layer wind flow could be maintained throughout the computational domain. We were satisfied that profiles of $U(z)$ and $k(z)$ at successive x -sections remain essentially unchanged from Eqs. (1) and (4) when flow passes through the computational domain. The second reference case was computation of wind flow over a low-rise building. Test conditions were identical to the study by AIJ (Tamura, *et al.* 1997, AIJ 1998). Computed results of wind flow pattern and wind pressure on building walls were found to fall within the ranges of variation of wind tunnel data and CFD data from numerous comparison studies in the AIJ project.

4.1. Pedestrian-level wind environment of a single tall building (Case I)

Fig. 3 shows the computed velocity vectors on the x - z plane in Case I. Data points shown have been interpolated from the denser mesh in the numerical model. Main features of experimental wind flow pattern are reproduced in the numerical solution. With wind incident on the front building wall, stagnation occurs at $z/H \approx 0.7$. Below this height, wind was brought towards the ground, as well as escaping around the side edges (which is shown by computed flow pattern on horizontal planes, not shown here). At upper levels, wind escapes over the top of building leading to flow separation on the roof. Behind the building, a large recirculating zone is found and it extends a distance about $2.5H$ downwind. Contours of total turbulent kinetic energy k are also shown in non-dimensional values of k/U_H^2 .

Downwind development of mean wind speed and turbulent kinetic energy on the x - z plane is shown in Fig. 4. Vertical profiles of $k(z)$ at successive x -stations shows that very high level of turbulence is created in the separated flow above the roof. There are high turbulence levels in the

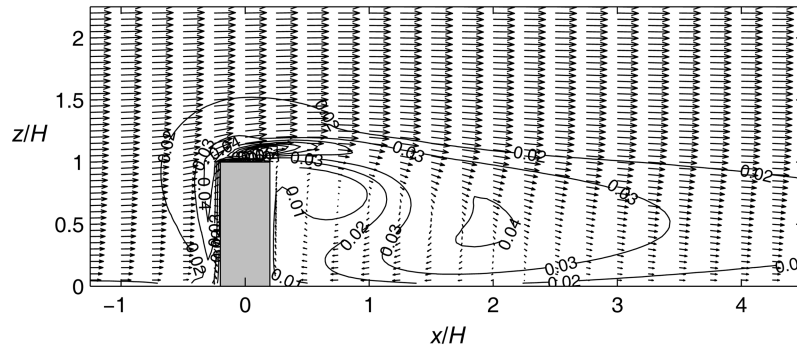


Fig. 3 Computed mean velocity vectors and contours of turbulent kinetic energy k/U_H^2 on x - z plane. Case I

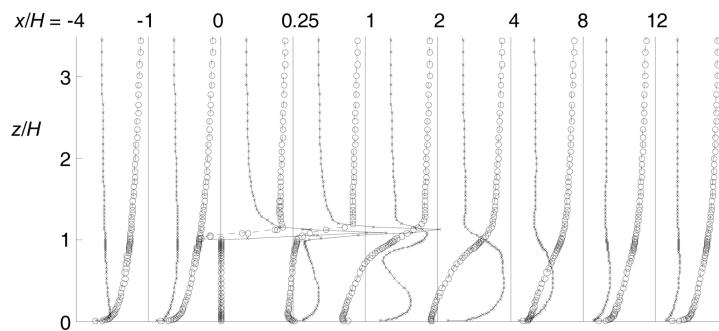


Fig. 4 Development of vertical profiles of mean wind speed (o) and turbulent kinetic energy (x) in flow past a building in Case I

building wake but downwind of the large recirculating zone, turbulent kinetic energy returns almost to the inlet level as expected. Profiles of $U(z)$ show recirculating flow behind the building. Downstream of $x/H > 8$, the profiles return to the inlet power law profile.

Flow patterns on horizontal planes across the building, not shown, show clearly escape of wind flow around the building corners. Wind pressures on building walls and roofs have been obtained in the CFD solution. Their values and distribution patterns agree well with past observations (e.g. Paterson and Apelt 1986). On the pedestrian-level plane at $z = 1$ cm, ground-level velocity vectors (U , V) are shown in Fig. 5. The vectors show clearly the presence of corner streams of high ground-level winds. Upper-level winds are brought to the ground by the front building wall to escape around the building corners. The vectors also show that some flow goes away from the front building wall on the ground level due to the standing vortex in front of the building (Melbourne and Joubert 1971).

Velocity vectors in Fig. 5 are shown at the computational grid points on the pedestrian-level plane. The data are plotted again in Fig. 6 on a regular grid of uniform spacing at $0.1B$ in both x and y directions. Shown in the lower half of the figure is our wind tunnel measurement data from To and Lam (1995a). They were obtained with a split-fibre hot-film probe on the same measurement grid. Both results show the corner flow streams as the most noticeable features of pedestrian-level wind environment (Melbourne and Joubert 1971). In the wake region right behind the building, wind tunnel data of To and Lam (1995a) show low-speed vectors flowing downwind

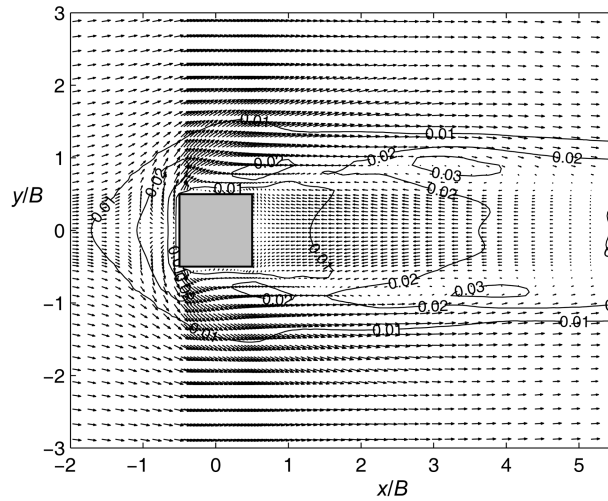


Fig. 5 Computer velocity vectors and contours of turbulent kinetic energy k/U_H^2 on pedestrian level. Case I

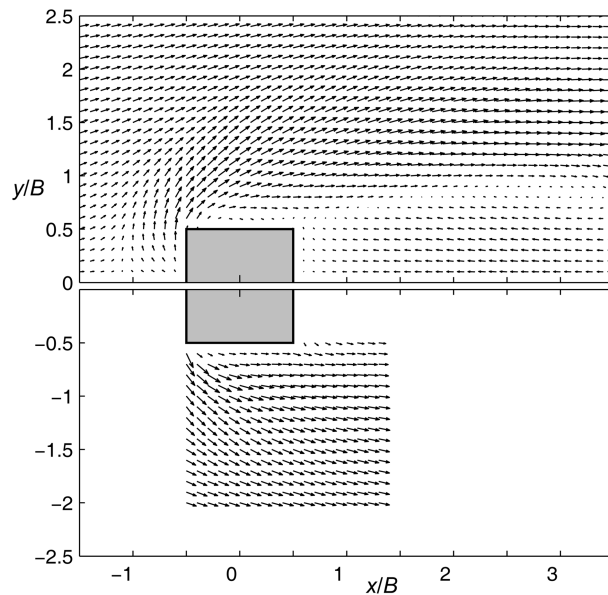


Fig. 6 Mean velocity vectors on pedestrian level (Case I). Upper: CFD results; Lower: wind tunnel experiments

on the ground level. The split-fibre probe in that study was aligned in a way to distinguish to which lateral direction the mean flow vector points. In that setting, the probe could not distinguish backward flow vectors. The present CFD results show the more reasonable low-speed backward flow towards the rear side of building. In this study, we have carried out flow visualizations using thread tufts and found that mean reverse flow exists on the pedestrian level behind the building. Thus, flow vector data of To and Lam (1995a) at regions behind buildings are not used in this paper.

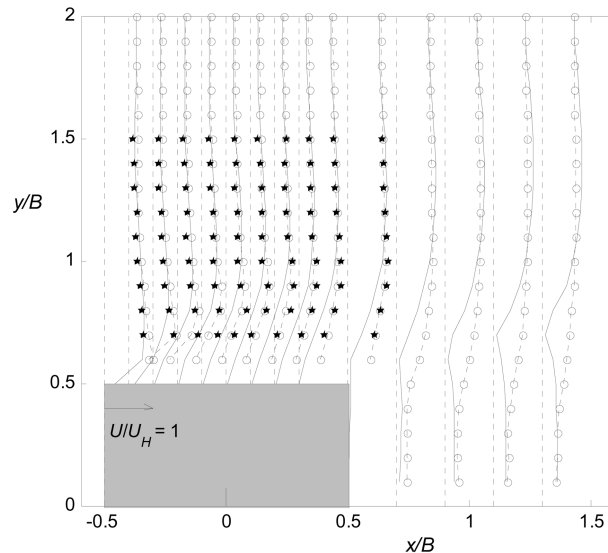


Fig. 7 Comparison of CFD and wind tunnel data of pedestrian-level wind speeds (Case I). Solid lines: CFD; °: corrected wind tunnel data of To & Lam (1995a); filled symbols: present measurements with 7-hole probe

In our re-examination of the ground-level wind speed measurement data of To and Lam (1995a,b), we found that there had been an error during the conversion of wind speed data to their non-dimensional form of U/U_H . The reference wind speed at roof height of building had been wrongly reduced by a constant. The wind tunnel data now shown in Fig. 6 have been corrected accordingly. In preparing this paper, we also repeated measurement of ground-level wind speed at some points using a 7-hole probe (Aeroprobe Inc.). Fig. 7 shows the comparison of magnitudes of ground-level wind speeds between CFD and the corrected wind tunnel data of To and Lam (1995a). Data of present measurement are also included and they support the validity of the previous wind tunnel data. For CFD data, magnitudes of pedestrian-level wind speeds are calculated from the computed horizontal velocity components as:

$$U_{PL} = \sqrt{U^2 + V^2} \quad (7)$$

To avoid complexity, the symbol U will be used to denote U_{PL} in future discussion.

It can be observed in Fig. 7 that at regions laterally away from the building, ground-level wind speeds from CFD and wind tunnel have values close to the free-field value at $U/U_H \approx 0.6$ (for an atmospheric boundary layer of mean wind speed profile described by a power law of exponent 0.15). On going towards the building, pedestrian-level wind speed increases because of the corner stream. Around the lateral side of the building, wind speeds in the corner stream from the wind tunnel have higher values than the CFD predictions. The same observation is made at regions close to the building sidewall. The corner stream predicted by CFD, however, extends beyond the building. In regions of $x/B \geq 0.7$ and $y/B > 1$, wind speeds significantly higher than the free-field value are predicted by CFD but this is not found in the wind tunnel data.

Fig. 8 compares CFD results and wind tunnel data in form of contours of ground-level wind

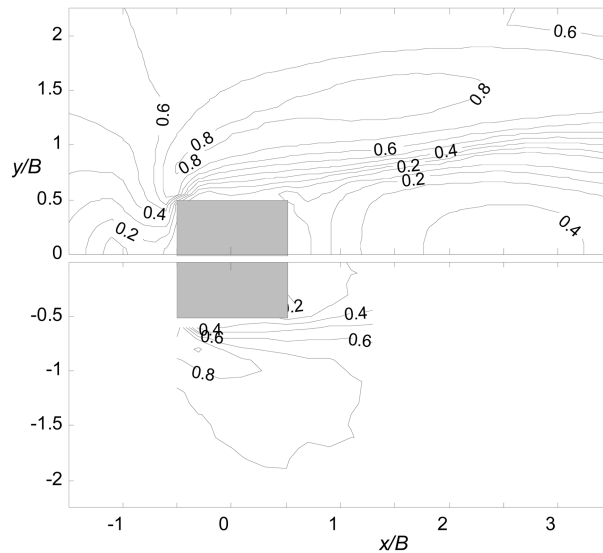


Fig. 8 Distribution of pedestrian-level wind speeds U/U_H (Case I). Upper: CFD results; Lower: wind tunnel experiments

speed. Comparing the two sets of wind speed contours, it is observed that in the wind tunnel, very high pedestrian-level wind speeds occur just around the building corner and then wind speeds inside the corner stream decrease significantly downstream. For the corner stream computed by CFD, ground-level wind speeds remains high at $U/U_H > 0.8$ over a long downstream distance extending more than two building breadths. Another difference is that the corner stream in CFD is aligned more laterally away from the building. Figs. 6-8 also show that in the wind tunnel, flows close to the building sidewalls have higher wind speeds than in CFD.

Being a RANS-based turbulence model, the $k-\varepsilon$ model is known to perform poorly in flows with strongly curving streamlines and tends to average out spatial flow variations. For upper-level winds to reach the pedestrian level, the streamlines change directions sharply a few times. It is thus not surprising that in the computation, build-up of high wind speeds on the pedestrian level needs a longer development distance. In the wind tunnel, very high pedestrian-level wind speeds could be reached just around the building corners. The numerical model, however, cannot reproduce this high velocity gradient in the streamwise direction.

Qualitatively, CFD computation succeeds in reproducing key features of environmental wind conditions. The sheltered region behind the building is computed to have a calm wind environment. Large wind speed gradients are experienced when pedestrians come out of the sheltered zone across the downwind line along building sidewalls. The computation shows presence of high-speed corner flow streams and region of moderate pedestrian-level wind speeds in front of building due to the standing vortex. However, alignment of the corner streams and location of highest ground-level wind speeds inside the corner streams are not well predicted by CFD. This problem is particularly relevant in the present flow configuration where the tall building is located without any significant surrounding buildings. In most reported CFD studies of pedestrian-level winds around actual building developments, the target building is surrounded by many neighbouring buildings and corner streams of high pedestrian-level winds are mostly channelled to flow along building gaps or

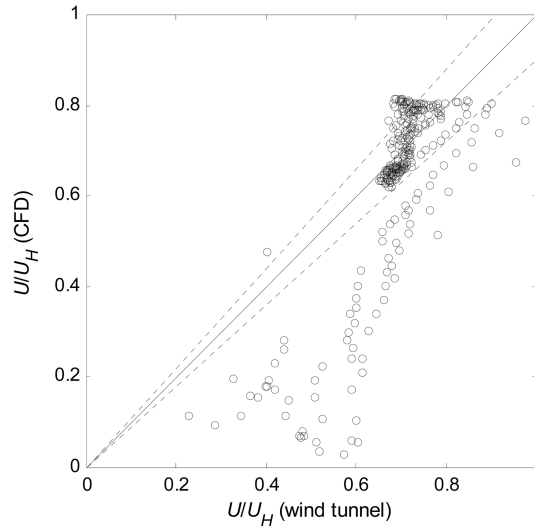


Fig. 9 Comparison of ground-level wind speeds between CFD and wind tunnel data at wind tunnel measurement points (Case I). Lines of 1:1 and $\pm 10\%$

regions among adjacent buildings (e.g. He and Song 1999, Ferreira, *et al.* 2002).

Fig. 9 shows scatter plot of ground-level wind speeds obtained by CFD against those in wind tunnel at the wind tunnel measurement points in Fig. 6. In regions close to the building sidewalls, CFD data are much lower than wind tunnel results. In the corner stream of high pedestrian-level wind speeds, CFD data and wind tunnel data agree with each other within $\pm 10\%$. Differences in alignment of corner streams and locations of highest wind speed inside the streams between CFD and wind tunnel data is responsible for the irregular pattern of the scatter plot around higher levels of U/U_H . In CFD, highest ground-level wind speeds at $U/U_H > 0.8$ are computed over the long corner stream (Fig. 7) but those locations in the wind tunnel have wind speeds dropping from $U/U_H \approx 0.85$ to 0.7. For the corner stream from wind tunnel data, ground-level wind speeds remains high at $U/U_H > 0.7$ over large downstream and lateral distances. In CFD, wind speeds inside the corresponding region vary widely between $0.6 < U/U_H < 0.8$.

To investigate the boundary condition effect of inlet turbulence intensity profile on the numerical results, we have repeated CFD computation with $I_u(z)$ decreased by 20% from Eq. (2) as well as increased by 20%. With lower turbulence intensity in incident wind flow, distribution pattern of ground-level wind speed computed on pedestrian level is very similar to that in Fig. 8. The corner stream of $U/U_H > 0.8$ extends a slightly longer downstream distance with the highest wind speed reached farther downstream. Results at the higher turbulence intensity level case, Case I-a, are shown in the upper part of Fig. 10. They show some slightly different features from the original Case I. The corner stream is computed to have a wider width right around the corner and highest ground-level wind speeds are reached at more upstream locations. The sensitivity test suggests that turbulence intensity levels higher than actual values may slightly help to bring up the slow development of corner stream in the CFD model. We also repeat computation of Case I with a mean wind speed profile of more urban type terrain. In this Case I-b, an exponent of 0.27 is used instead of 0.15 in Eq. (1) for the mean wind speed profile at inlet. Computed contours of U/U_H are shown in Fig. 10. Under the steeper profile of $U(z)$, significantly lower levels of U/U_H are

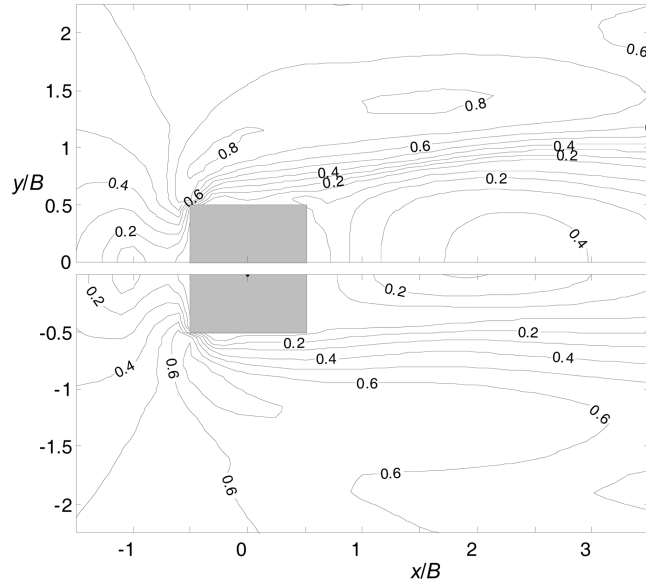


Fig. 10 Distribution of pedestrian-level wind speeds U/U_H . Upper: Case I-a, higher inlet turbulence intensities; Lower: Case I-b, mean wind speed profile of urban terrain

computed in the corner stream. Development of the corner stream is faster than Case I. Some other differences such as the narrower sheltered zone behind the building are observed. The same urban-type profile, with power law exponent 0.27, is used in Yoshie, *et al.* (2005a) in which wind speeds at height $z=0.125B$ around a 1:1:2 building model were measured in the wind tunnel as well as computed by CFD. The two sets of results in that study were found to fall within $\pm 10\%$ from each other. The highest wind speeds reaching on the plane $z=0.125B$ were measured to have values about $U/U_H \approx 0.8$.

Wind vectors and speeds shown in Figs. 6-8 are mean horizontal velocity components (U , V). To examine the significance of vertical velocity component W , a scatter plot comparing values of W to pedestrian-level wind speed U_{PL} is shown in Fig. 11 for all computational grid points on the

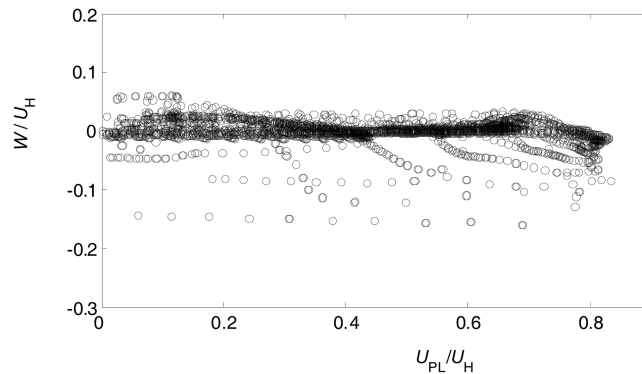


Fig. 11 Scatter plot of mean vertical velocity components against pedestrian-level wind speeds (Case I)

pedestrian level. The results show that at most points, the vertical flow component has very small mean values. It is justified to assume that mean wind flow on the pedestrian level is horizontal. This supports the use of a single hot-wire or a split-fibre probe for measurement of pedestrian-level wind speeds in the wind tunnel. There are, however, some points where W has negative values up to $W/U_H = -0.15$. An examination of the distribution of W on the pedestrian level shows that these downward flow components occur mainly in the standing vortex region and in the corner streams. In the standing vortex region, downward velocity component has average values about $W/U_H \approx -0.1$ with peak values reaching $W/U_H = -0.15$ in front of the building. Horizontal wind speed in this region has values about $U/U_H \approx 0.2$. The vertical flow component is thus important in this region.

In addition to mean wind speeds, gust wind speeds on the ground level are equally important in the assessment of pedestrian-level wind environment. Gust wind speeds may be estimated from mean wind speeds and r.m.s. values of wind speed fluctuations. The split-fibre probe data in the wind tunnel provide r.m.s. fluctuations of horizontal wind vector. The present CFD solutions include turbulent kinetic energy k . Using Eqs. (3) and (4), it is possible to estimate r.m.s. wind speed on the pedestrian level as:

$$\sigma_U \approx \sqrt{\sigma_u^2 + \sigma_v^2} = \sqrt{1.71k} \quad (8)$$

Fig. 12 shows the comparison of σ_U/U_H between CFD results and wind tunnel data. Again, the numerical model cannot predict the fast generation of turbulence in the corner flow stream. Wind tunnel data shows a peak region of high $\sigma_U/U_H > 0.2$ just around the upwind building corner but in CFD, a peak region is found more downstream outside the downwind building corner with lower levels of $\sigma_U/U_H > 0.18$.

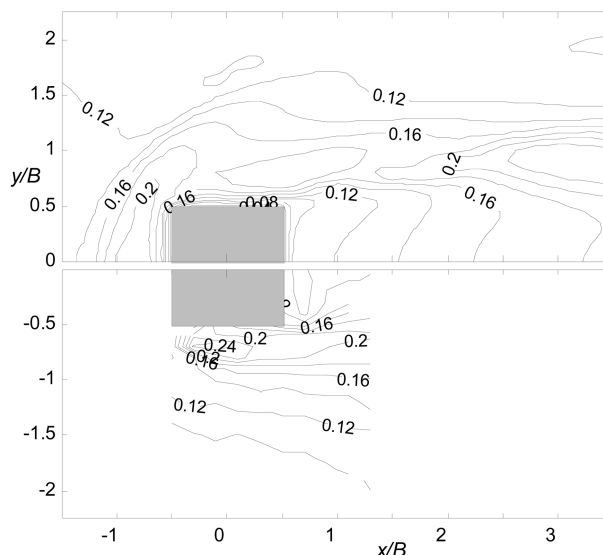


Fig. 12 Contours of r.m.s. wind speed fluctuations σ_U/U_H on pedestrian level (Case I). Upper: CFD results; Lower: wind tunnel experiments

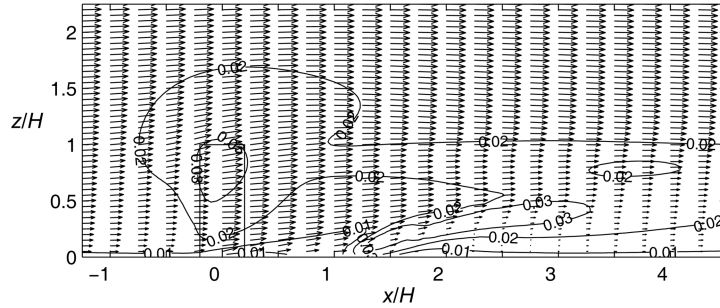


Fig. 13 Mean velocity vectors and contours of turbulent kinetic energy k/U_H^2 on x - z plane through center of building gap (Case II)

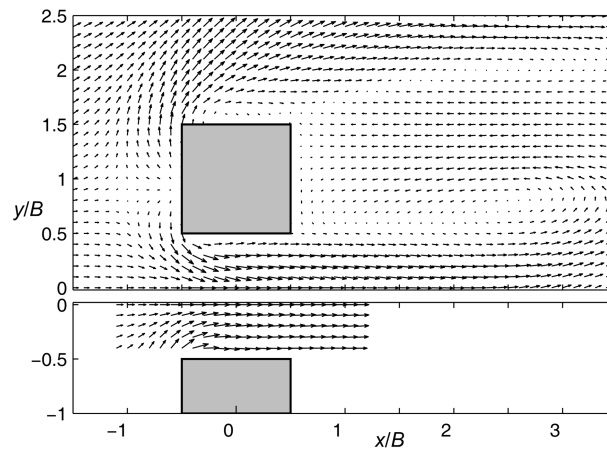


Fig. 14 Wind vectors on pedestrian level (Case II). Upper: CFD results; Lower: wind tunnel experiments

4.2. Wind normal to a row of buildings (Case II)

For Case II, Fig. 13 shows the wind flow pattern on the x - z plane cutting through the center of gap between two buildings. In the wake behind each building member, the computed results, not presented here, show similar pattern as that in Fig. 3. Here in Fig. 13, the vectors show that wind flow is channeled through the gap and that wind speeds in the gap are higher than the incoming values. Contours of k/U_H^2 show that the accelerated flow inside the gap has low turbulence levels and that high turbulence is found where downstream ends of the recirculating zones behind two buildings meet.

Fig. 14 presents comparison of pedestrian-level velocity vectors between CFD and the corrected wind tunnel data of To and Lam (1995a). Both sets of vectors show that wind flow is channeled into the building gap and subsequently exit in form of a high-speed air stream. Similar flow patterns are observed on other horizontal planes at different heights. Contour plots of wind speed are shown in Fig. 15. Wind tunnel results show that the building gap is covered by uniformly high pedestrian-level wind speeds with the highest speed contours at $U/U_H > 0.9$. In CFD, the development of channeled gap flow is more gradual with lower ground-level wind speeds alongside building walls and at center of gap. Two corner streams of high pedestrian-level wind speed at $U/U_H > 0.9$ develop from upwind building corners and they merge slowly inside the building gap. Fig. 16 compares

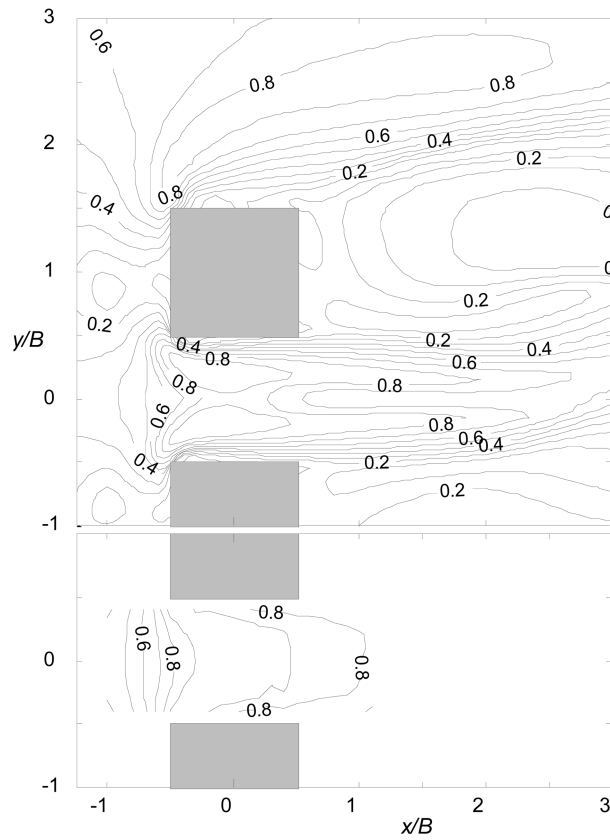


Fig. 15 Contours of pedestrian-level wind speeds U/U_H (Case II). Upper: CFD results; Lower: wind tunnel experiments

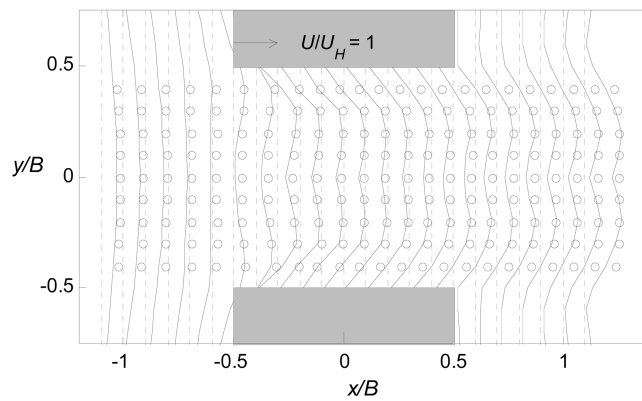


Fig. 16 Comparison of CFD and wind tunnel data of pedestrian-level wind speeds (Case II). Solid lines: CFD; °: corrected wind tunnel data of To & Lam (1995a)

pedestrian-level wind speeds inside the building gap between CFD and wind tunnel measurement. In general, the two sets of data agree within $\pm 10\%$ but it is evident that CFD under-predicts the

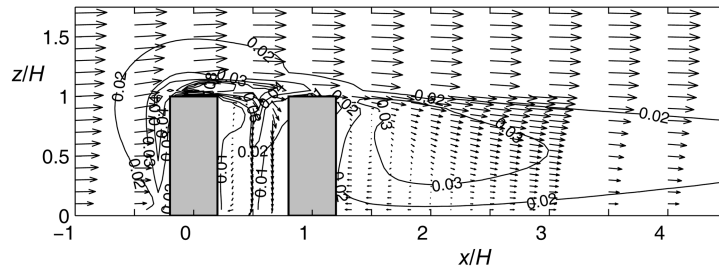


Fig. 17 Flow past two buildings (Case III): velocity vectors and contours of turbulent kinetic energy k/U_H^2 on x - z plane

high wind speed along centerline of the gap.

For r.m.s. wind speed fluctuations, CFD and wind tunnel data compare well with each other (data not shown for brevity). Turbulence levels inside the central part of the building gap have values of $\sigma_U/U_H < 0.15$. These values are lower than those on the free side of the building. This is due to suppression of turbulence generation as wind flow is channeled through the building gap.

4.3. Wind blowing along a row of buildings (Case III)

Fig. 17 shows the computed flow over two buildings in Case III on the x - z plane. Flow over and around the upstream building is very similar to that of an isolated building. Flow separation is observed on the roof with high level of turbulence generation. In the region between buildings, there exists large-scale low-speed flow recirculation. Negligible roof separation occurs on the downstream building and this leads to a reduction in size of the large recirculating flow region behind this building. For an isolated building, the recirculating flow region extends to $2.5H$ behind the building (Fig. 3). Here, it only covers less than $1.5H$ behind the downstream building. Furthermore, lower levels of turbulent kinetic energy are found inside the region. Computed flow vectors on the horizontal planes, not shown here, show that the downstream building is sheltered completely by the upstream building. The downstream building is surrounded by low speed flow in the wake of upstream building and no separation is observed around the sidewalls of downstream building.

Contours of pedestrian-level wind speeds are shown in Fig. 18. Sheltering effect on the downstream building can also be observed. Both wind tunnel and CFD results show the absence of corner streams around the downstream building. Flow pattern around the upstream building is very similar to that of an isolated building (Fig. 8). This suggests that presence of the downstream building does not lead to significant difference in the pedestrian-level wind environment of the upstream building. Similar observation is made on the contours of r.m.s. wind speed fluctuations which are not shown for brevity. Scatter plot of CFD and wind tunnel data of ground-level wind speeds is similar to that in Fig. 9. In corner streams of the upwind building, ground-level wind speeds from CFD and wind tunnel are in good agreement within $\pm 10\%$.

4.4. Wind blowing along a row of buildings in diamond arrangement (Case IV)

For Case IV, wind tunnel data are available from To and Lam (1995b). Computation is also made on a single building with wind blowing along the diagonal of building plan form. Fig. 19 shows the pedestrian-level wind vectors computed for the two cases. High ground-level wind speeds are

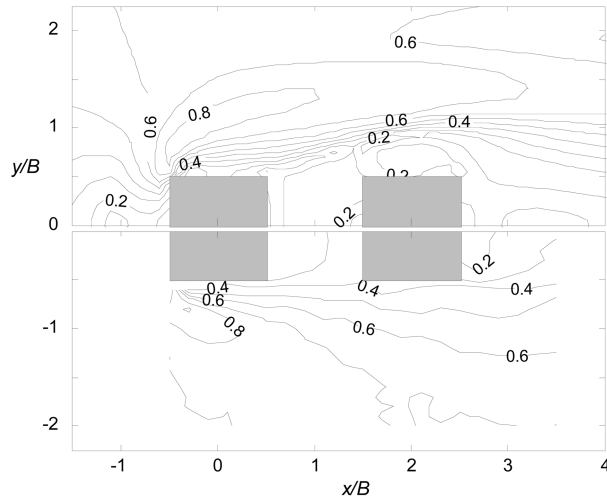


Fig. 18 Contours of pedestrian-level wind speeds U/U_H (Case III). Upper: CFD results; Lower: wind tunnel experiments.

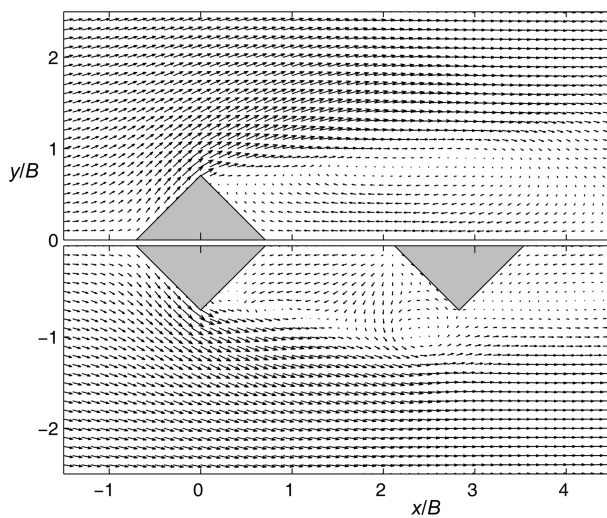


Fig. 19 CFD wind vectors on pedestrian level around row of two buildings in diamond arrangement (Case IV). Upper: one single building; Lower: two buildings in line to flow

mainly found in the corner streams around the single or the first building in the row. No standing vortex is observed in front of this building. Areas around the second building, and the more downstream buildings in the row as expected, are sheltered with no corner stream present. However, a recirculating flow region is observed in front of each windward corner of the second building. The upper half of Fig. 19 shows that without the downstream building, there is reverse flow on the pedestrian level behind the single building at $x/B < 4$. It seems that presence of the second building strengthens this reverse flow into a vortex-like recirculating flow region on the ground level. It also appears that this vortex-like flow only exists close to the ground because velocity vectors on higher horizontal planes do not show such a well-established recirculating region.

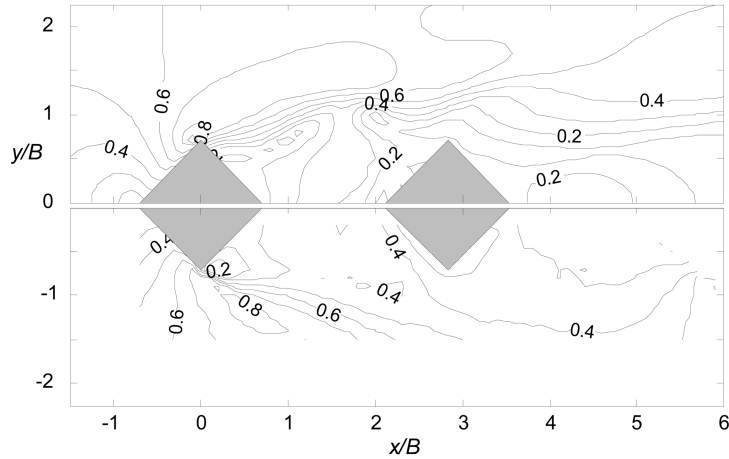


Fig. 20 Contours of pedestrian-level wind speeds U/U_H around row of two buildings in diamond arrangement (Case IV). Upper: CFD results; Lower: wind tunnel experiments

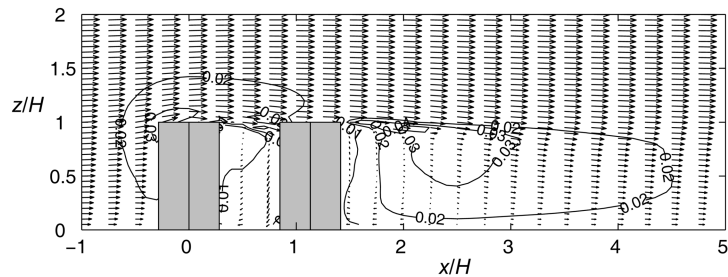


Fig. 21 Flow past row of two buildings in diamond arrangement (Case IV): velocity vectors and contours of turbulent kinetic energy k/U_H^2 on x - z plane

Fig. 20 shows the comparison of ground-level wind speed contours between numerical computation and wind tunnel measurements. Similar patterns of corner streams and sheltering by upwind building as Fig. 19 are observed. Although this orientation of the upwind building presents a large blockage area to the incoming flow, inclination of its two windward walls to incident wind flow facilitates more upper-level winds to flow along the walls and leave around the building corners before reaching the ground. This may explain why the highest pedestrian-level wind speeds computed inside the corner streams have lower levels than Case III (Fig. 18). From the scatter plot of wind speed data, CFD speeds are found to match wind tunnel values within $\pm 10\%$ at locations of high pedestrian-level wind speeds. Computed wind flow pattern on the x - z plane is shown in Fig. 21. The degree of sheltering offered by the upwind building is clearly shown. Comparing with Fig. 17, it is evident that much lower level of turbulence is found in roof separation.

5. Conclusions

In this paper, we attempt to evaluate the reliability of CFD technique in predicting pedestrian-level wind environment around a group of tall buildings. Accuracy of RANS-based CFD is assessed through direct comparison with wind tunnel data. The physical model consists of a row of identical

square tall buildings in a rather open exposure. We employed a finite-volume code and RNG $k-\varepsilon$ model for turbulence closure.

For a single tall building or the upwind building in a row, CFD reproduces the main features of pedestrian-level wind environment including presence of high-speed corner streams, standing vortex in front of building and leeward sheltered zone. However, there are differences in the alignment of corner streams to the building and the location of highest wind speeds inside the corner streams. Point-to-point comparison of wind speed data shows that at points of high wind speeds, CFD values match wind tunnel measurements within $\pm 10\%$. At locations close to the building sidewalls, very low ground-level wind speeds are predicted by CFD but significantly higher wind speeds were measured in the wind tunnel.

When wind blows normal to the building row, high-speed ground-level winds are found channeling through the building gap. CFD cannot produce the fast establishment of uniform high pedestrian-level wind speeds across the building gap. When the wind direction is along the building row, the upwind building offers nearly total protection to downwind building in terms of pedestrian-level wind environment. Both CFD and wind tunnel results show the absence of corner streams for downwind building due to sheltering.

This paper shows that CFD can be a useful tool for the evaluation of environmental wind conditions around tall buildings. In terms of magnitudes of higher ground-level wind speeds, agreement with wind tunnel data is within $\pm 10\%$. We note that CFD cannot allow fast development of high-speed flow regions or sharply bending regions. This may be due the tendency of $k-\varepsilon$ models to average out spatial variations of the flow. While more advanced CFD models may be able to improve the prediction, we believe that wind tunnel measurements at selected strategic locations should be used to supplement CFD results in an accuracy-demanding investigation.

Acknowledgements

The investigation is supported by two research grants awarded by the Research Grants Council of Hong Kong: HKU7014/02E and PolyU1/02C. Sensitivity tests in Fig. 10 on boundary conditions of wind characteristics in CFD models are carried out as result of helpful comments from the anonymous reviewer to which we owe sincere gratitude. The reviewer's query on the wind tunnel measurement data also leads us to re-examine the data and subsequently carry out the proper corrections.

References

- Architectural Institute of Japan (1998), "Numerical prediction of wind loading on buildings and structures", March 1998.
- Ferreira, A. D., Sousa, A. C. M., and Viegas, D. X. (2002), "Prediction of building interference effects on pedestrian level comfort", *J. Wind Eng. Ind. Aerodyn.*, **90**, 305-319.
- Fluent Inc. (2003), Fluent 6.1 User's Manual, www.fluent.com.
- He, J. and Song, C. C. S. (1999), "Evaluation of pedestrian winds in urban area by numerical approach", *J. Wind Eng. Ind. Aerodyn.*, **81**, 295-309.
- Irwin, H. P. A. H. (1981), "A simple omni-directional sensor for wind tunnel studies of pedestrian level winds", *J. Wind Eng. Ind. Aerodyn.*, **7**, 219-239.
- Isyumov, N. and Davenport, A. G. (1975), "The ground level wind environment in built up area", *Proceedings of 4th Int. Conf. Wind Effects on Buildings and Structures*, London, 403-422.
- Leonard, B. P. (1979), "A stable and accurate convective modelling procedure based on quadratic upstream

- interpolation”, *Comput. Method Appl. Mech. Eng.*, **19**, 59-98.
- Livesey, F., Morrish, D., Mikitink, M., and Isyumov, N. (1992), “Enhanced scour tests to evaluate pedestrian level winds”, *J. Wind Eng. Ind. Aerodyn.*, **41-44**, 2265-2276.
- Lu, W. Z., Lo, S. M., Fang, Z., and Yuen, K. K. (2001), “A preliminary investigation of airflow field in designated refuge floor”, *Build. Environ.*, **36**(2), 219-230.
- Melbourne, W. H. (1978), “Criteria for environmental wind conditions”, *J. Ind. Aerodyn.*, **3**, 241-249.
- Melbourne, W. H. and Jourbert, P. N. (1971), “Problem of wind flow at the base of tall buildings”, *Proceedings of 3rd Int. Conf. on Wind Effects on Buildings and Structures*, Tokyo, 105-114.
- Meroney, R. N., Leitl, B. M., Rafailidis, S., and Schatzmann, M. (1999), “Wind-tunnel and numerical modeling of flow and dispersion about several building shapes”, *J. Wind Eng. Ind. Aerodyn.*, **81**, 333-345.
- Murakami, S. (1998), “Overview of turbulence models applied in CWE-1997”, *J. Wind Eng. Ind. Aerodyn.*, **74-76**, 1-24.
- Patankar, S. V. (1980), *Numerical Heat Transfer and Fluid Flow*, Hemisphere Publ. Corp., Washington D.C.
- Paterson, D. A. and Apelt, C. J. (1986), “Computation of wind flows over buildings”, *J. Wind Eng. Ind. Aerodyn.*, **24**, 193-213.
- Sasaki, R., Uematsu, Y., Yamada M., and Saeki, H. (1992), “Application of infrared thermography and a knowledge-based system to the evaluation of the pedestrian-level wind environment around buildings”, *J. Wind Eng. Ind. Aerodyn.*, **67-68**, 873-883.
- Stathopoulos, T. and Storms, R. (1986), “Wind environmental conditions in passages between buildings”, *J. Wind Eng. Ind. Aerodyn.*, **24**, 19-31.
- Stathopoulos, T. and Wu, H. Q. (1995), “Generic models for pedestrian-level winds in built-up regions”, *J. Wind Eng. Ind. Aerodyn.*, **54-55**, 515-525.
- Straw, M. P., Baker, C. J., and Robertson A. P. (2000), “Experimental measurements and computations of the wind-induced ventilation of a cubic structure”, *J. Wind Eng. Ind. Aerodyn.*, **88**, 213-230.
- Tamura, T., Kawai, H., Kawamoto, S., Nozawa, K., Sakamoto, S., and Ohkuma, T. (1997), “Numerical prediction of wind loading on buildings and structures-Activities of AIJ cooperative project on CFD”, *J. Wind Eng. Ind. Aerodyn.*, **67-68**, 671-685.
- To, A. P. and Lam, K. M. (1995a), “Evaluation of pedestrian-level wind environment around a row of tall buildings using a quartile-level wind speed descriptor”, *J. Wind Eng. Ind. Aerodyn.*, **54-55**, 527-541.
- To, A. P. and Lam, K. M. (1995b), “Pedestrian-level wind environment around a row of tall buildings in diamond arrangement”, *Proceedings of 9th Int. Conf. on Wind Engineering*, New Delhi, 2034-2042.
- Tominaga, Y., Yoshie, R., Mochida, A., Kataoka, H., Harimoto, K., and Nozu, T. (2005), “Cross comparisons of CFD prediction for wind environment at pedestrian level around buildings. Part 2: Comparison of results for flow-field around building complex in actual urban area”, *Proceedings of 6th Asia-Pacific Conference on Wind Engineering*, Seoul, September.
- Uematsu Y., Yamada, M., Higashiyama H., and Orimo T. (1992), “Effects of the corner shapes of high-rise buildings on the pedestrian-level wind environment with consideration for mean and fluctuating wind speeds”, *J. Wind Eng. Ind. Aerodyn.*, **41-44**, 2289-2300.
- Van Doornaal, J. P. and Raithby, G. D. (1984), “Enhancement of the SIMPLE method for predicting incompressible fluid flows”, *Numer. Heat Transfer.*, **7**, 147-163.
- Yakhot, V. and Orszag, S. A. (1986), “Renormalization-group analysis of turbulence”, *Phys. Rev. Lett.*, **57**, 1722-1724.
- Yoshie, R., Mochida, A., Tominaga, Y., Kataoka, H., Harimoto, K., Nozu, T., and Shirasawa, T. (2005a), “Cooperative project for CFD prediction of pedestrian wind environment in the Architectural Institute of Japan”, *Proceedings of 4th European & African Pacific Conference on Wind Engineering*, Prague, July.
- Yoshie, R., Mochida, A., Tominaga, Y., Kataoka, H., and Yoshikawa, M. (2005b), “Cross comparisons of CFD prediction for wind environment at pedestrian level around buildings. Part 1: Comparison of results for flow-field around a high-rise building located in surrounding building blocks”, *Proceedings of 6th Asia-Pacific Conference on Wind Engineering*, Seoul, September.
- Zhou, Y. and Stathopoulos, T. (1997), “A new technique for the numerical simulation of wind flow around buildings”, *J. Wind Eng. Ind. Aerodyn.*, **72**, 137-147.